International Journal of Thermofluids 19 (2023) 100371

Contents lists available at ScienceDirect

International Journal of Thermofluids

journal homepage: www.sciencedirect.com/journal/international-journal-of-thermofluids

Influence of PST and PHF heating conditions on the swirl flow of Al+Mg+TiO_2 ternary hybrid water-ethylene glycol based nanofluid with a rotating cone

Yousef Salah [a], Osama Al Mukbel [a], Yaman Sabsabi [a], S. Saranya [a], Qasem M. Al-Mdallal [a,*], Farzona Mukhamedova [b]

[a] Department of Mathematical Sciences, UAE University, P.O. Box 15551, Al-Ain, United Arab Emirates
[b] Mathematics Institute, University of Warwick, Coventry CV4 7AL, United Kingdom

ARTICLE INFO

Keywords:
Shifted Legendre collocation method
Ternary hybrid nanofluid
Rotating cone
Free convection
Prescribed surface temperature
Prescribed heat flux

ABSTRACT

Swirl flow heat exchangers are commonly used in industrial processes such as power generation, chemical processing, and refrigeration. They can be used for both heating and cooling applications and can be designed to handle a wide range of fluid flow rates and temperatures. This study investigated the influence of PST (prescribed surface temperature) and PHF (prescribed heat flux) heating conditions on the swirl flow of Al+Mg+TiO_2 ternary hybrid water-ethylene glycol (50/50) based nanofluid with a heated rotating cone. The governing ordinary differential equations were derived from the partial differential equations using the proper similarity transformations. The problem was solved using the Shifted Legendre Collocation Method (SLCM), which is a powerful numerical method. The results showed that the PST heating conditions had a significant impact on the flow and heat transfer characteristics of the ternary hybrid nanofluid. Under PHF heating conditions, the swirl velocity distribution was leading to a noteworthy influence. The use of the Al+Mg+TiO_2 ternary hybrid water-ethylene glycol based nanofluid resulted in a significant enhancement in the convective heat transfer coefficient. The SLCM method provided accurate and efficient numerical solutions for the problem, demonstrating its suitability for simulating complex fluid flow and heat transfer problems.

1. Introduction

Ternary hybrid nanofluids have received significant attention in recent years due to their superior heat transfer performance compared to traditional fluids. They exhibit a higher thermal conductivity and convective heat transfer coefficient, which can lead to significant improvements in heat transfer efficiency in various applications. Ternary hybrid nanofluids are nanofluids formed out of three distinct sorts of nanoparticles dissolved in a base fluid. These nanoparticles can be metallic, oxide, or carbon-based, and are chosen based on their ability to enhance the thermal and/or transport properties of the fluid. Applications of ternary hybrid nanofluids include but are not limited to, heat exchangers, automotive radiators, solar collectors, electronic cooling systems, and biomedical devices. These applications benefit from the nanofluid's improved heat exchange efficiency, which leads to improved system efficiency and performance. Recently, Sahoo [1] investigated the heat transfer and flow characteristics of a radiator filled with various nanoparticle-based ternary hybrid nanofluids. Nanoparticles, namely aluminum oxide (Al_2O_3), copper oxide (CuO), and graphene oxide (GO) in distilled water, were involved in this experimental study. The heat transfer coefficient, friction factor, and pressure drop of the nanofluids inside a car radiator were measured, and it was found that the hybrid nanofluids with a combination of Al_2O_3, CuO, and GO exhibited better thermo-hydraulic performance compared to binary and single nanoparticle-based nanofluids. The study also found that the shape of the nanoparticles played an important role in determining the heat transfer performance of the nanofluids. Cao et al. [2] aimed to study the behavior of the nanofluid under different levels of partial slip. The authors investigated the dynamics of a ternary-hybrid nanofluid consisting of a colloidal mixture of water and various nanoparticles with different shapes and sizes. The authors found that the size and shape of the nanoparticles affected the nanofluid's flow behavior, with larger and irregularly shaped nanoparticles causing more turbulence and flow

Abbreviations: THNF, Ternary Hybrid Nanofluid; SLCM, Shifted Legendre Collocation Method; PST, Prescribed Surface Temperature; PHF, Prescribed Heat Flux.

* Corresponding author.
E-mail address: q.almdallal@uaeu.ac.ae (Q.M. Al-Mdallal).

https://doi.org/10.1016/j.ijft.2023.100371

Available online 11 May 2023

Nomenclature

B	Magnetic field intensity, $kgs^{-2}A^{-1}$
C_{fx}	Skin friction coefficient
C_p	Specific heat, $Jkg^{-1}K^{-1}$
f	Dimensionless tangential velocity
g_r	Acceleration due to gravity, ms^{-2}
Gr	Grashof number
k	Thermal conductivity, $Wm^{-1}K^{-1}$
L	Reference length, m
M	Magnetic parameter
θ	Dimensionless fluid temperature
Nu_x	Local Nusselt number
Pr	Prandtl number of base fluid
q_w	Wall heat flux, Wm^{-2}
Re	Local Reynolds number
r	Dimensionless radius
g	Dimensionless swirl velocity
T_r	Reference temperature, K
T_w	Temperature at the cone surface, K
T_∞	Ambient temperature, K
T	Temperature, K
u	x-component of dimensionless velocity
U	Reference velocity, ms^{-1}
v	y-component of dimensionless velocity
w	θ-component of dimensionless velocity
x	Dimensionless coordinate measured along the surface
y	Dimensionless coordinate normal to the surface

Greek Letters

α	Thermal diffusivity, m^2s^{-1}
β	Thermal expansion coefficient, K^{-1}
ε	Spin parameter, -
ϕ	Volume fraction of nanoparticles, -
γ	Half of vertex angle
μ	Dynamic viscosity, $kgm^{-1}s^{-1}$
ν	Kinematic viscosity, m^2s^{-1}
σ	Electric conductivity, Sm^{-1}
ρ	Density, kgm^{-3}
ω	Angle of rotation
Θ	Dimensionless temperature ratio
ψ	Stream function, -
τ_w	Wall shear stress, Nm^{-2}

Subscripts

Thnf	Hybrid nanofluid
bf	Base fluid
Al, TiO_2, *MgO*	Solid nanoparticles
∞	Edge of the boundary layer

Superscript

$(.)'$	Differentiation with respect to y

instability. Said et al. [3] examined the synthesis, stability, density, and viscosity of aluminum oxide (Al_2O_3), zinc oxide (ZnO), and copper oxide (CuO) with ethylene glycol-based ternary hybrid nanofluids. The authors aimed to evaluate the performance of the nanofluids as heat transfer fluids and to develop models for predicting their thermophysical properties using modern machine learning techniques. The outcomes demonstrated that the density and viscosity of the nanofluids were significantly enhanced by the addition of nanoparticles. In comparison to binary and single nanoparticle-based nanofluids, hybrid nanofluids with a combination of Al_2O_3, ZnO, and CuO displayed better stability and thermophysical properties. Adun et al. [4] demonstrated that the use of optimized ternary hybrid nanofluids can improve the thermodynamic performance and reduce the environmental impact of an integrated solar power generation system with storage capacities. They found that the use of optimized ternary hybrid nanofluids could increase the efficiency of the system by up to 16% compared to the base fluid. Furthermore, the environmental impact analysis showed that the use of the optimized nanofluids reduced the emission of greenhouse gasses and other pollutants. This is because the improved efficiency of the system allowed for a reduction in the amount of fuel needed to generate the same amount of power. Shao et al. [5] used numerical simulations to investigate the heat transfer characteristics and flow behavior of the ternary hybrid nanofluid under natural convection conditions. They found that the use of the nanofluid significantly enhanced the heat transfer performance of the enclosure, with a maximum enhancement of 16.5% compared to the base fluid. Moreover, it was found that the movement of the hot baffles improved the fluid mixing and resulted in a more effective cooling performance. Shahzadi et al. [6] presents a study on the use of fractional ternary nanofluids to alter the blood stream in an oblique stenosed aneurysmal artery with slip conditions. They discovered that the use of the nanofluid can significantly change the blood flow's velocity profile and wall shear stress, potentially improving the way aneurysms are treated. Wang et al. [7] presented a study on the use of ternary hybrid nanofluids to enhance the cooling performance of a flat confined loop thermosyphon for electronic devices cooling and found that the use of the nanofluids significantly enhanced the heat transfer performance of the thermosyphon, with a maximum enhancement of 16.2% compared to the base fluid. Numerous researchers have investigated ways to increase the rate of heat transfer and the cooling effect while taking into account various geometries and configurations ([8–11]).

In many engineering applications, including chemical engineering, aerospace engineering, and power generation, fluid flow over a rotating cone is a typical phenomenon. In many industrial processes, the rotating cone is a tool for mixing, heat transfer, and particle separation. A rotating cone's fluid flow is a complicated phenomenon that involves the interaction of the fluid flow and cone rotation (Tien and Campbell [12]). The flow field and the properties of heat transfer are impacted by the secondary flow created by the cone's rotational induction of a centrifugal force. Depending on the rotational speed and the flow rate, the flow over a rotating cone may be laminar or turbulent. There are numerous useful practical applications for the study of fluid flow over rotating cones. For instance, rotating cones are used as mixing devices in chemical reactors in chemical engineering to increase the effectiveness of chemical reactions. In aerospace engineering, the performance of turbomachinery, such as turbines and compressors, is improved by studying the flow over a rotating cone (Banerjee et al. [13]). In steam turbine blades, the flow over a rotating cone is used to increase the efficiency of energy conversion in power generation. Due to their improved heat transfer qualities, nanofluids have recently drawn more attention when used in fluid flow over a rotating cone. Important implications for the creation of more effective heat transfer devices in various industrial applications can be drawn from research on nanofluid flow over rotating cones ([14–21]). Saranya et al. [22] provided the valuable insights into the behavior of ferrofluids in free convection flows over a heated spinning cone. Mainly it was observed that the performance of hybrid ferrofluid was in highest levels when compared to regular fluid and mono type ferrofluids. Hakeem et al. [23] investigated the effects of transverse magnetic fields on the flow of hybrid nanofluids over a vertical rotating cone, where the base fluid could be either Newtonian or non-Newtonian. The results showed that increasing magnetic field strength results in increased skin friction and heat

transfer coefficients. Additionally, the non-Newtonian base fluid had a more significant impact on the flow than the Newtonian fluid. An examination of the heat transfer properties of a magnetohydrodynamic nanofluid flow composed of moving, oxytactic microorganisms and nanoparticles in three dimensions was done by Mogharrebi et al. [24]. It was understood that motile microorganisms can be incorporated into nanofluid to improve heat transfer and prevent particle aggregation. With consideration for Hall current and the thermal jump condition, the quadratic convection flow of water carrying hybrid nanoparticles of Ag (25 nm) and MgO (40 nm) about a rotating cone exterior was considered by Rana and Gupta [25]. Here are some recent studies relating to flow over rotating cone (see Khan et al. [26], Hussain et al. [27] and Nazir et al. [28]).

Fluid flow and heat transfer with Prescribed Surface Temperature (PST) and Prescribed Heat Flux (PHF) heating conditions are important areas of research in the field of thermal engineering. Prescribed Surface Temperature (PST) is a boundary condition where the temperature at the surface of a solid is known and fixed. This condition is commonly encountered in many practical applications such as heat exchangers, electronic cooling systems, and thermal energy storage systems. In these systems, the temperature of the solid surface is maintained at a certain level to ensure proper heat transfer and to avoid any damage due to overheating. Prescribed Heat Flux (PHF) is a boundary condition where the amount of heat transferred through the surface of a solid is known and fixed. This condition is often encountered in applications such as electric heating elements, laser heating, and solar collectors. In these systems, the heat flux is controlled to achieve a desired level of heating. The study of fluid flow and heat transfer with PST and PHF heating conditions has important practical applications. In heat exchangers, the PST condition is used to maintain a constant temperature difference between the hot and cold fluids. In electronic cooling systems, the PST condition is used to maintain a constant temperature at the surface of electronic components to avoid overheating. In solar collectors, the PHF condition is used to control the amount of heat absorbed by the collector to maximize energy conversion. Thus, PST and PHF heating conditions is important for understanding the behavior of thermal systems under different boundary conditions. Frequently, the effects of PST and PHF on fluid flow and heat transfer were investigated by numerous researches using different numerical simulations and experimental techniques. A thorough analysis of the transient boundary layer MHD flow of a non-Newtonian micropolar Fe_3O_4–Ag hybrid nanofluid mixed with uniformly sized conducting dust nanoparticles throughout a stretching sheet, considering PST and PHF cases, was presented by Nabwey and Mahdy [29]. Eid and Mabood [30] numerically studied the entropy impact on MHD micropolar dusty nanofluid flowing over a stretching permeable sheet using Darcy-Forchheimer model. Ahmed et al. [31] evaluated the power-law heat/mass fluxes for Williamson nanofluid flows over a nonlinear bidirectional elongating surface with PST and PHF heating conditions. Mostafazadeh et al. [32] observed the natural convective heat transfer in the laminar flow of nanofluid in a vertical channel. The authors used both single-phase and two-phase approaches to analyze the behavior of the nanofluid under different conditions, including the radiation with PST and PHF boundary conditions. The behavior of magnetized hybrid nanofluid under radiative bidirectional flow with prescribed thermal activity (PST and PHF), using the Keller-Box approach was explored by Ahmad et al. [33]. An analytical estimation of energy dissipation in viscoelastic fluid flow phenomena over a deformable surface, taking into account viscous, Joulian, and Darcy dissipations along with PST and PHF conditions were presented by Bhukta et al. [34].

From the above overview, it follows that the study of the nature of swirl flow ternary hybrid nanofluid under the influence of PST and PHF heating condition with a rotating cone has received relatively little attention, despite the fact that numerous investigations have been conducted on various aspects of swirl flow over a rotating cone. As a result, the subject of the paper under discussion is the interaction of PST and PHF heating conditions and swirl flow of ternary hybrid nanofluid of Al, Mg, TiO_2 with water-ethylene glycol at the surface of a rotating cone. The proposed concept is compared and analyzed under both PST and PHF heating conditions. Ternary hybrid nanofluids have the potential to revolutionize various industries by improving the efficiency of heat transfer systems, reducing energy consumption, and increasing sustainability. Overall, the study highlights the importance of considering the heating conditions when designing and analyzing heat transfer systems using ternary hybrid nanofluids. The use of hybrid nanofluids and advanced numerical methods like SLCM can further improve the efficiency and performance of such systems.

2. Problem formulation

We take into account the incompressible, laminar, steady flow of a ternary hybrid nanofluid in a boundary layer as well as the free convection heat transfer from the rotating heated cone. Fig. 1 depicts the 2D theoretical formulation and curvilinear coordinate system of a heated rotating cone placed in a still ternary hybrid nanofluid, which has a radius, $\breve{r}$, rotating around its axis. With the cone inverted, the slant height and the $\breve{x}$-axis, which run along the cone's surface, and the $\breve{y}$-axis, which run in the normal direction, respectively, coincide with the slant height of the cone. The vertical cone is thought to be rotating with a steady angular velocity, Ω (= constant), and the angular position is denoted by, ω.

Applying a consistent external magnetic field B along the $\breve{y}$-axis, it is presumed that the induced magnetic field pales in comparison to the applied magnetic field under the assumption of a low magnetic Reynolds number, additionally supposing that the flow is non-dissipative and axisymmetric, respectively. The no-slip condition is considered along the fluid-solid interface, alongside an understanding that the base fluid as well as solid nanoparticles remain in thermal equilibrium (see Ece [35], Aghamajidi et al. [36] and Saranya et al. [22]).

$$\frac{\partial}{\partial \breve{x}}(\breve{r}\breve{u}) + \frac{\partial}{\partial \breve{y}}(\breve{r}\breve{v}) = 0, \tag{1}$$

$$\breve{u}\frac{\partial \breve{u}}{\partial \breve{x}} + \breve{v}\frac{\partial \breve{u}}{\partial \breve{y}} - \frac{\breve{w}^2}{\breve{x}} = \nu_{Thnf}\frac{\partial^2 \breve{u}}{\partial \breve{y}^2} + \frac{(\rho\beta)_{Thnf}}{\rho_{Thnf}} g_r \cos\gamma (T - T_w) - \frac{\sigma B^2\ \breve{u}}{\rho_{Thnf}}, \tag{2}$$

$$\breve{u}\frac{\partial \breve{w}}{\partial \breve{x}} + \breve{v}\frac{\partial \breve{w}}{\partial \breve{y}} + \frac{\breve{u}\breve{w}}{\breve{x}} = \nu_{Thnf}\frac{\partial^2 \breve{w}}{\partial \breve{y}^2} - \frac{\sigma B^2\ \breve{w}}{\rho_{Thnf}}, \tag{3}$$

$$\breve{u}\frac{\partial T}{\partial \breve{x}} + \breve{v}\frac{\partial T}{\partial \breve{y}} = \alpha_{Thnf}\frac{\partial^2 T}{\partial \breve{y}^2}. \tag{4}$$

The boundary conditions applied to the current model are:

$$\left.\begin{array}{l} \breve{u}(\breve{x},\ \breve{y}) = 0, \quad \breve{v}(\breve{x},\ \breve{y}) = 0, \quad \breve{w}(\breve{x},\ \breve{y}) = \breve{r}\ \Omega, \\ \text{PST}: \ T(\breve{x},\ \breve{y}) = P(\breve{x}), \quad \text{PHF}: -k_{bf}\dfrac{\partial T}{\partial \breve{y}} = Q(\breve{x}), \end{array}\right\} \quad \text{at} \quad \breve{y} = 0, \tag{5}$$

$$\breve{u}(\breve{x},\ \breve{y}) \to 0, \quad \breve{w}(\breve{x},\ \breve{y}) \to 0, \quad T(\breve{x},\ \breve{y}) \to T_\infty, \quad \text{as} \quad \breve{y} \to \infty. \tag{6}$$

Additionally, the dimensionless variables listed below are presented as tools that can facilitate the similarity analysis.

$$\begin{array}{l} \breve{x} = xL, \quad \breve{y} = yLGr^{-\frac{1}{4}}, \quad \breve{u} = uU, \quad \breve{v} = vUGr^{-\frac{1}{4}}, \quad \breve{w} = w\Omega L, \\ \breve{r} = rL, \quad T = T_\infty + \Theta T_r, \end{array} \tag{7}$$

where, the velocity components along the $\breve{x}$, $\breve{y}$, and ω directions are denoted by $\breve{u}$ $\breve{v}$ and $\breve{w}$, respectively. $\breve{r} = \breve{x}\sin\gamma$, denotes the cone's bottom radius; γ is the semi vertex angle. g_r denotes the acceleration due

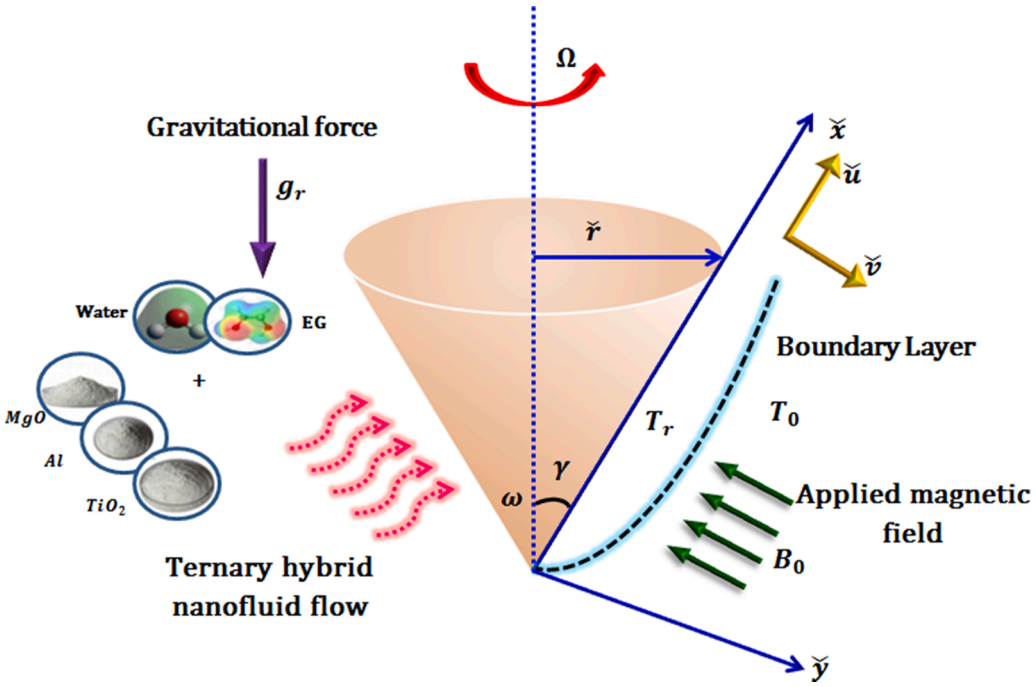

Fig. 1. Physical model of the system.

to gravity. β denotes the thermal expansion coefficient. L denote the reference length. Furthermore, some significant dimensionless parameters are given in Table 1 (Ece [35], Aghamajidi et al. [36] and Saranya et al. [22]).

The non-dimensional parameters shown in Table 1 are substituted into Eqs. (1) - (4) to produce the following results:

$$\frac{\partial}{\partial x}(ru)+\frac{\partial}{\partial y}(rv)=0, \tag{8}$$

$$u\frac{\partial u}{\partial x}+v\frac{\partial u}{\partial y}-\frac{Re^2}{Gr}\frac{w^2}{x}=\frac{C_4}{C_5}\frac{1}{\phi}\frac{\partial^2 u}{\partial y^2}+C_{11}\Theta-\frac{1}{C_5}M\Gamma^2 u, \tag{9}$$

$$u\frac{\partial w}{\partial x}+v\frac{\partial w}{\partial y}+\frac{uw}{x}=\frac{C_4}{C_5}\frac{1}{\phi}\frac{\partial^2 w}{\partial y^2}-\frac{1}{C_5}M\Gamma^2 w, \tag{10}$$

$$u\frac{\partial \Theta}{\partial x}+v\frac{\partial \Theta}{\partial y}=\frac{C_{10}}{C_9}\frac{1}{\phi}\frac{1}{Pr}\frac{\partial^2 \Theta}{\partial y^2}. \tag{11}$$

The coefficients C_i for $i=1, 2, ..., 11$ are defined in Appendix 1, these coefficients represent the models of viscosity, thermal conductivity, heat capacity and thermal expansion coefficient implemented for platelet, spherical, and cylindrical nanoparticles, where the model for these thermophysical properties are followed from the works of Sahoo [1] and Xiu et al. [37]. The numerical values for these thermophysical properties for respective base fluid and nanoparticles are described in detail in Table 2.

After applying the dimensionless parameters, the appropriate conditions for boundaries displayed by Eqs. (5), (6) and (7) are finally as follows:

$$\left.\begin{array}{l} u(x,y)=0,\quad v(x,y)=0,\quad w(x,y)=r, \\ \text{PST}:\ \Theta(x,y)=p(x),\quad \text{PHF}:\dfrac{\partial\Theta}{\partial y}=-q(x), \end{array}\right\} \quad \text{at} \quad y=0, \tag{12}$$

$$u(x,y)\to 0,\quad w(x,y)\to 0,\quad \Theta(x,y)\to 0\,,\quad \text{as}\quad y\to\infty. \tag{13}$$

where, $p(x)=\frac{P(\breve{x})-T_\infty}{T_w-T_\infty}$ and $q(x)=\frac{Q(\breve{x})L}{k_f(T_w-T_\infty)}\frac{1}{Gr^4}$. By creating the stream function, Ψ, we put the similarity analysis into practice. The velocity components (u, v) in dimensionless form are connected to the stream function by $ru=\frac{\partial\Psi}{\partial y}$, $rv=-\frac{\partial\Psi}{\partial x}$.

Now, the boundary layer variables have been established as follows:

$$\Psi(x,y)=xrf(y),\quad w=rg(y),\quad \Theta=x\theta(y), \tag{14}$$

where, the similarity variable $f(y)$ denotes tangential velocity; the

Table 1
Non-dimensional parameters and their expression.

Mathematical expression	Name of the parameter
$U=(g_r\cos\gamma\ \beta L(T_w-T_\infty))^{\frac{1}{2}}$	Reference velocity
$Gr=\left(\frac{UL}{\nu_{bf}}\right)^2$	Grashof number
$B=B_0\frac{b(x)}{r\sqrt{1-r'^2}}$	Magnetic field intensity
$\Gamma=\frac{b(x)}{r\sqrt{1-r'^2}}$	Magnetic field function
$Pr=\frac{\nu_{bf}}{\alpha_{bf}}$	Prandtl number
$Re=\frac{\Omega L^2}{\nu_{bf}}$	Rotational Reynolds number
$M=\frac{\sigma_f B_0^2 L}{U\ \rho_{bf}}$	Magnetic parameter
$\varepsilon=\frac{Re^2\sin^2\gamma}{Gr}$	Spin parameter

Table 2
Thermo-physical properties of base fluid and nanoparticles (Xiu et al. [37] and Saranya et al. [22]).

Properties	Water-ethylene glycol (Base fluid)	*Al*	TiO_2	*MgO*
$\rho(kgm^{-3})$	1056	2702	4250	3580
$C_p(Jkg^{-1}K^{-1})$	3288	903	686.2	960
$k(Wm^{-1}K^{-1})$	0.425	237	8.954	48.4
Pr	29.86	–	–	–
$\beta(K^{-1})$	0.00341×10^{-5}	25×10^{-6}	8.5×10^{-6}	21×10^{-6}
Shape	–	Platelet	Spherical	Cylindrical

Table 3
Validation of $f'(0)$ and $-\theta'(0)$ (PST); $\theta(0)$ (PHF) with Ece [35] at Pr = 1; $\phi_{Al} = 0.0$; $\phi_{TiO_2} = 0.0$; $\phi_{MgO} = 0.0$.

ε	M	Ece [35]				Present work			
		PST		PHF		PST		PHF	
		$f'(0)$	$-\theta'(0)$	$f'(0)$	$-\theta'(0)$	$f'(0)$	$\theta(0)$	$f'(0)$	$\theta(0)$
0.0	0.0	0.681502	0.638866	0.891689	1.431129	0.681483	0.638852	0.891691	1.431130
	1.0	0.559759	0.558693	0.809136	1.562934	0.559761	0.558691	0.809142	1.562940
	2.0	0.486789	0.503384	0.758532	1.671318	0.486806	0.503352	0.758543	1.671333
0.5	0.0	0.846506	0.671948	1.025288	1.388947	0.846488	0.671936	1.025290	1.388949
	1.0	0.685479	0.581380	0.913967	1.529816	0.685481	0.581379	0.913972	1.529820
	2.0	0.590029	0.519667	0.847058	1.644361	0.590047	0.519638	0.847071	1.644374
1.0	0.0	1.001960	0.700534	1.155920	1.351701	1.001943	0.700522	1.155923	1.351703
	1.0	0.808193	0.602564	1.018019	1.498813	0.808196	0.602564	1.018025	1.498818
	2.0	0.692037	0.535364	0.935287	1.618506	0.692053	0.535337	0.935299	1.618519

similarity variable $g(y)$ denotes the swirl velocity; and the similarity variable $\theta(y)$ denotes the temperature, respectively. It is understood that the applied magnetic field strength is constant across the cone wall when $\Gamma = 1$. Added to that, the transformations in Eq. (14) fulfill the requirement for continuity Eq. (8), so Eqs. (9) - (11) take the simplified forms shown below.

$$\frac{C_4}{C_5}\frac{1}{\phi}f''' + \left[2ff'' - f'^2 + \varepsilon g^2\right] + C_{11}\theta - \frac{1}{C_5}Mf' = 0, \tag{15}$$

$$\frac{C_4}{C_5}\frac{1}{\phi}g'' + [2fg' - 2f'g] - \frac{1}{C_5}Mg = 0, \tag{16}$$

$$\frac{C_{10}}{C_9}\frac{1}{\phi}\theta'' + Pr[2f\theta' - f'\theta] = 0, \tag{17}$$

The corresponding boundary conditions in Eqs. (12) and (13) take the following forms:

$$f(0) = 0, \quad f'(0) = 0, \quad g(0) = 1,$$

$$\text{PST case}: \quad \theta(0) = \frac{p(x)}{x}, \text{PHF case}: \theta'(0) = -\frac{q(x)}{x}, \tag{18}$$

$$f'(\infty) = 0, \; g(\infty) = 0, \theta(\infty) = 0. \tag{19}$$

To enable a similarity solution, each function connected to the PST and PHF boundary conditions described by Eq. (18) must be equatable to constant. The $p(x)$ and $q(x)$ functions seem to be proportional to x in this way. The ratios $p(x)/x$ and $q(x)/x$ are capable of being set to unity without losing generality. For specialized proportionality constant values, this may be done by selecting the reference temperature T_r. As a result, the boundary conditions for PST and PHF in Eq. (18) can be expressed as:

$$\text{PST case}: \quad \theta(0) = 1, \quad \text{PHF case}: \quad \theta'(0) = -1. \tag{20}$$

The local skin friction coefficient and the local Nusselt number are two engineering-relevant parameters that have non-dimensional forms as follows:

$$C_{fx} = \frac{2\tau_w}{\rho_{bf}U^2} \text{ and } Nu_x = \frac{Lq_w}{k_{bf}(T_w - T_\infty)}, \tag{21}$$

where the wall shear stress τ_w and the wall heat flux q_w are represented by

$$\tau_w = \mu_{Thnf}\left(\frac{\partial \breve{u}}{\partial \breve{y}}\right)_{\breve{y}=0}, \quad q_w = -k_{Thnf}\left(\frac{\partial T}{\partial \breve{y}}\right)_{\breve{y}=0}. \tag{22}$$

The local Nusselt number, Nu_x, and skin friction coefficient, C_{fx}, can be expressed using non-dimensional parameters as follows (see Ece [35]):

$$\frac{Gr^{\frac{1}{4}}}{x}C_{fx} = \frac{C_4}{\phi}\,2F''(0), \tag{23}$$

$$\begin{aligned} &\text{PST Case}: \quad \frac{Gr^{-\frac{1}{4}}}{x}\,Nu_x = -\frac{C_9}{\phi}\theta'(0), \\ &\text{PHF Case}: \quad \frac{Gr^{-\frac{1}{4}}}{x}\,Nu_x = \frac{C_9}{\phi}\,\frac{1}{\theta(0)}. \end{aligned} \tag{24}$$

3. Numerical approach

Numerical calculations are achieved by using the Shifted Legendre Collocation Method (SLCM). It is based on the Legendre polynomial approximation of the solution, which is shifted to create a set of collocation points in the interval of interest. These collocation points are used to construct a system of algebraic equations, which are then solved to obtain an approximation to the solution of the differential equation. The well-known closed forms of the Legendre polynomials $\mathscr{L}_n(t)$ of degree n on the interval $[-1, 1]$ are represented by (see Saranya et al. [38])

$$\mathscr{L}_n(t) = \sum_{\kappa=0}^{n}\binom{n}{\kappa}\binom{n+\kappa}{\kappa}\left(\frac{t-1}{2}\right)^{\kappa}. \tag{25}$$

Let $\{\mathscr{L}_0, \mathscr{L}_1, \ldots\}$ be the shifted Legendre polynomials (LPs). These LPs are orthogonal over $[-1, 1]$ with weighting function $w(t) = 1$ and satisfy

$$\int_0^1 \mathscr{L}_n(t)\mathscr{L}_m(t)\,dt = \frac{2\delta_{n,m}}{2n+1}, \qquad n, m \in \mathbb{N}, \tag{26}$$

where, the Kronecker delta, $\delta_{n,m}$, as is expressed as:

$$\delta_{n,m} = \begin{cases} 0, & \text{if } n \neq m, \\ 1 & \text{if } n = m. \end{cases}$$

Since $[0, y_\infty)$ is the domain for the Eqs. (15) - (17), then the shifted LPs should be on $[0, y_\infty)$. Thus, by setting $y = \frac{y_\infty + y_\infty t}{2}$ gives

$$\mathscr{L}_n^*(y) = \mathscr{L}_n\left(\frac{2y}{y_\infty} - 1\right), \qquad y \in [0, y_\infty). \tag{27}$$

For the sake of convenience, we may rewrite Eqs. (15) - (17) in the following forms:

$$f''' + \phi\left\{\frac{C_5}{C_4}\left[2ff'' - f'^2 + \varepsilon g^2\right] + \frac{C_5C_{11}}{C_4}\theta - \frac{1}{C_4}Mf'\right\} = 0, \tag{28}$$

$$g'' + \phi\left\{\frac{C_5}{C_4}[2fg' - 2f'g] - \frac{1}{C_4}Mg\right\} = 0, \tag{29}$$

$$\theta'' + \phi\left\{\frac{C_9}{C_{10}}Pr[2f\theta' - f'\theta]\right\} = 0, \tag{30}$$

subject to

$$\begin{aligned} &f(0) = e_1, \quad f'(0) = e_2, \quad f'(\infty) = e_3, \quad g(0) = e_4, \quad g(\infty) = e_5 \\ &\theta(0) = e_6(\text{PST}), \quad \theta'(0) = e_7(\text{PHF}), \quad \theta(\infty) = e_8. \end{aligned} \tag{31}$$

In relation to the shifted LPs, the functions $f(y)$, $g(y)$ and $\theta(y)$ can be expressed as below (Saranya et al. [38]):

$$f(y) \approx Z_f(y) = \sum_{i=0}^{N+1} a_K \mathscr{L}^*_K(y), \tag{32}$$

$$g(y) \approx Z_g(y) = \sum_{i=0}^{N+1} d_K \mathscr{L}^*_K(y), \tag{33}$$

$$\theta(y) \approx Z_\theta(y) = \sum_{i=0}^{N+1} s_K \mathscr{L}^*_K(y), \tag{34}$$

where $\{a_\kappa\}_{\kappa=0}^{N+1}$, $\{d_\kappa\}_{\kappa=0}^{N+1}$ and $\{s_\kappa\}_{\kappa=0}^{N+1}$ are the Legendre coefficients that are to be determined. The residuals related to Eqs. (28)-(30) respectively, are given by:

$$R_f(y) = Z_f^{'''} + \frac{C_5}{C_4}\phi\left[2Z_f Z_f'' - Z_f'^2 + \varepsilon Z_g^2\right] - \frac{C_5 C_{11}}{C_4}\phi Z_\theta - \frac{1}{C_4}\phi M Z_f', \tag{35}$$

$$R_g(y) = Z_g'' + \frac{C_5}{C_4}\phi\left[2Z_f Z_g' - 2Z_f' Z_g\right] - \frac{1}{C_4}\phi M Z_g, \tag{36}$$

$$R_\theta(y) = Z_\theta'' + \frac{C_9}{C_{10}}\phi Pr\left[Z_f Z_\theta' - Z_f' Z_\theta\right], \tag{37}$$

The undefined coefficients $\{a_K\}_{K=0}^{N+1}$ are estimated by making the residuals $R_f(y)$ given in Eq. (35) vanish at the collocation points. The assumed collocation points are $y_j = y_0 + jh$; where, $j = 1, 2, 3, \ldots, N-2$, and $h = \frac{y_\infty - y_0}{N+1}$ is the uniform step size.

Furthermore, the boundary condition related to $f(y)$ given by Eq. (31) take the following form

$$f(0) = e_1, \Rightarrow \sum_{i=0}^{N+1} a_K \mathscr{L}^*_K(0) - e_1 := 0, \tag{38}$$

$$f'(0) = e_2, \Rightarrow \sum_{i=0}^{N+1} a_\kappa \left(\mathscr{L}^*_K(0)\right)' - e_2 := 0, \tag{39}$$

$$f'(y_\infty) = e_3, \Rightarrow \sum_{i=0}^{N+1} a_K \left(\mathscr{L}^*_K(y_\infty)\right)' - e_3 := 0, \tag{40}$$

Similarly, the undefined coefficients , $\{d_K\}_{K=0}^{N+1}$ and $\{s_K\}_{K=0}^{N+1}$ are estimated by making the residuals $R_g(y)$ and $R_\theta(y)$ given in Eqs. (36) and (37) vanish at the collocation points, y_j for $j = 1, 2, 3, \ldots, N-1$. The boundary conditions related to $g(y)$ and $\theta(y)$ are given as:

$$g(0) = e_4, \Rightarrow \sum_{i=0}^{N+1} d_k \mathscr{L}^*_K(0) - e_4 := 1, \tag{41}$$

$$g(y_\infty) = e_5, \Rightarrow \sum_{i=0}^{N+1} d_k \mathscr{L}^*_K(y_\infty) - e_5 := 0, \tag{42}$$

$$\text{PST Case}: \ \theta(0) = e_6, \Rightarrow \sum_{i=0}^{N+1} s_K \mathscr{L}^*_K(0) - e_6 := 0, \tag{43}$$

$$\text{PHF Case}: \ \theta'(0) = e_7, \Rightarrow \sum_{i=0}^{N+1} s_K \left(\mathscr{L}^*_K(0)\right)' - e_7 := 0, \tag{44}$$

$$\theta(y_\infty) = e_8, \Rightarrow \sum_{i=0}^{N+1} s_K \mathscr{L}^*_K(y_\infty) - e_8 := 0, \tag{45}$$

In short, the following algebraic equation system which is comprised of $3N + 6$ equations with $3N + 6$ unknowns need to be solved, to determine the unknown coefficients $\{a_\kappa\}_{K=0}^{N+1}$, $\{d_K\}_{K=0}^{N+1}$ and $\{s_K\}_{K=0}^{N+1}$.

$$\mathbf{Q}(\mathbf{V}) = \begin{bmatrix} \mathbf{F}(\mathbf{V}) \\ \mathbf{G}(\mathbf{V}) \\ \mathbf{H}(\mathbf{V}) \end{bmatrix} := 0, \tag{46}$$

where, $\mathbf{V} = [a_0, a_1, \ldots, a_{N+1}, d_0, d_1, \ldots, d_{N+1}, s_0, s_1, \ldots, s_{N+1}]^T$ is used to represent all the unknowns and the vectors $\mathbf{F(V)} = [\mathbf{F}_0, \mathbf{F}_1, \ldots, \mathbf{F}_{N+1}]^T$, $\mathbf{G(V)} = [\mathbf{G}_0, \mathbf{G}_1, \ldots, \mathbf{G}_{N+1}]^T$ and $\mathbf{H(V)} = [\mathbf{H}_0, \mathbf{H}_1, \ldots, \mathbf{H}_{N+1}]^T$ are defined as follows:

$$\boldsymbol{F}_0 = Z_f(0) - e_1; \mathbf{F}_j = R_f(y_j), \quad j = 1, \ldots, N-2; \mathbf{F}_N = Z_f'(0) - e_2; \mathbf{F}_{N+1} = Z_f'(y_\infty) - e_3,$$

$$\mathbf{G}_0 = Z_g(0) - e_4; \mathbf{G}_j = R_g(y_j), \quad j = 1, \ldots, N-1; \mathbf{G}_{N+1} = Z_g(y_\infty) - e_5,$$

$$\mathbf{H}_0 = \begin{cases} Z_\theta(0) - e_6 \ (\text{PST}), \\ Z_\theta'(0) - e_7 \ (\text{PHF}). \end{cases}; \mathbf{H}_j = R_\theta(y_j), \quad j = 1, \ldots, N-1; \ \mathbf{H}_{N+1} = Z_\theta(y_\infty) - e_8.$$

The multi-dimensional version of Newton's method is used for solving (46) by application of the functional iteration process, developed from choosing $\mathbf{V}^0$ and generating, for $\varepsilon \geq 1$,

$$\mathbf{V}^\epsilon = \boldsymbol{V}^{\epsilon-1} - \mathbf{J_Q}\left(\mathbf{V}^{\epsilon-1}\right)^{-1}\mathbf{Q}\left(\mathbf{V}^{\epsilon-1}\right), \tag{47}$$

where we represent the Jacobian matrix $\mathbf{Q}$ by $\mathbf{J_Q(V)}$. It is really significant to note here that the quadratic convergence of a Newton multi-dimensional method is possible if

i) $\| \mathbf{J}_\mathbf{Q}^{-1} \leq \mathscr{M}, \|$ where $\mathscr{M} > 0$, and the norm of the inverse of the Jacobian at $\mathbf{V}^\varepsilon$ is bounded.
ii) $\|\mathbf{J}(z_2) - \mathbf{J}(z_1)\| \leq \|z_2 - z_1,\|$ the Jacobian is Lipschitz continuous.

4. Result and discussion

This section presents the graphical illustrations of the physical constraints on tangential velocity profile ($f'(y)$), swirl velocity profile ($g(y)$), and temperature profile ($\theta(y)$). Moreover, this study examines two situations, namely: (a) PST; (b) PHF. The PST case is shown by solid lines, whereas PHF case is shown by dashed lines. Default values of the parameters for the all the calculations and graphs are $M = 0.2$; $\Gamma = 1.0$; $\varepsilon = 0.5$; $Pr = 29.86$; $\phi_{Al} = 0.01$; $\phi_{TiO_2} = 0.01$; $\phi_{MgO} = 0.01$. To verify the physical model, the records as of Ece [35] intended for a fluid devoid of nanoparticles with our findings are contrasted. For various magnetic and spin parameter values for PST and PHF boundary conditions, the values of the skin friction coefficient and heat transfer rate are shown in Table 3, respectively. As can be seen, there is a great fit in between the results from the present study and Ece [35].

We also validated the method by comparing our tangential velocity with the data published by Ece [35]. He investigated the flow created by a rotating cone in regular fluid. The set of coupled second-order nonlinear differential equations for $f'(y)$, $g(y)$ and $\theta(y)$ which are subject to the boundary conditions were solved numerically using the Thomas algorithm. The velocity pattern of the current investigation in comparison to data [35] is shown in Fig. 2. As can be observed, the results of the current study are consistent with the results (data points) across the whole range of y.

4.1. Discussion on tangential velocity profile

It is worth observing in Fig. 3 that, rising of the value of the spin parameter is capable of improving the tangential profile of the ternary hybrid nanofluid either the heating conditions is PST or PHF. As shown in Fig. 3, increasing the magnitude of ε implies increasing the rotation of the spinning cone, which increases the tangential fluid velocity because of the centrifugal force acting on the fluid. As the cone rotates faster, the

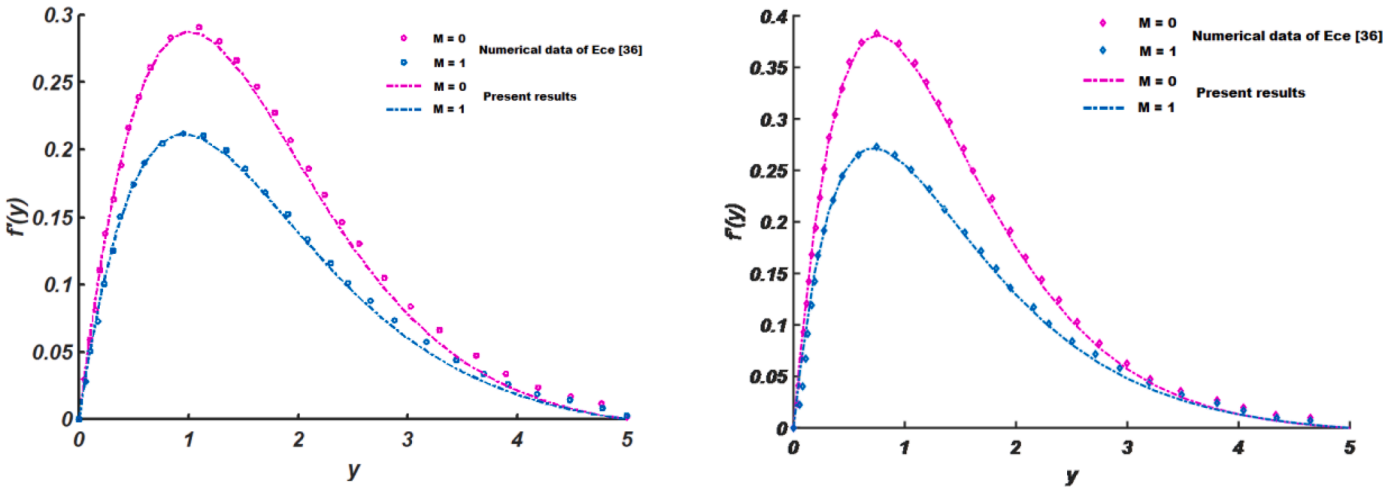

Fig. 2. Comparison of present results for tangential velocity $f'(y)$ with numerical results of Ece [35] at spin parameter (a) $\varepsilon = 0$ and (b) $\varepsilon = 1$ for different values of M.

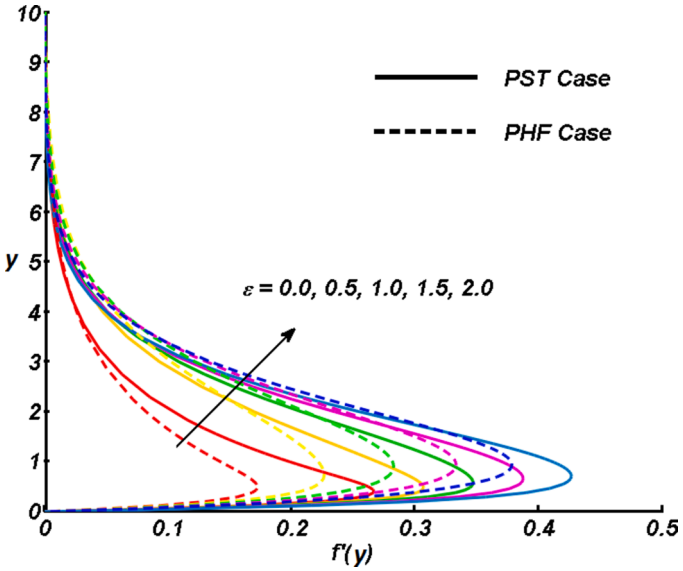

Fig. 3. Influence on tangential velocity by of spin parameter.

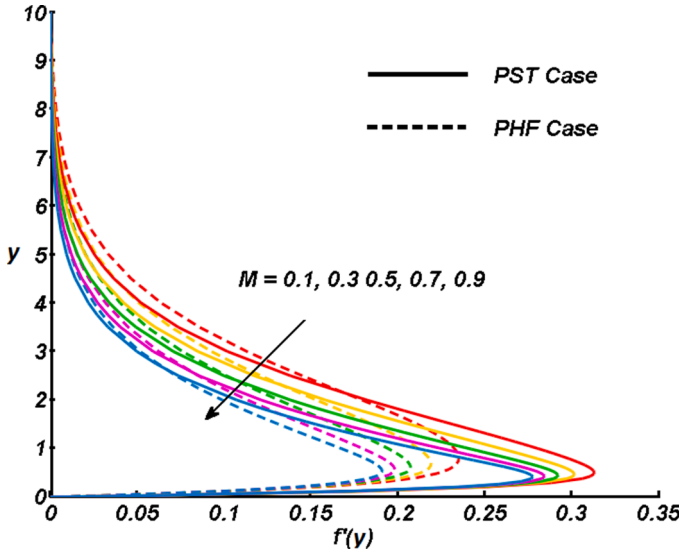

Fig. 4. Influence on tangential velocity by magnetic parameter.

fluid near the surface of the cone experiences an outward force due to the centrifugal force. This results in the fluid moving tangentially along the cone's surface, increasing the tangential velocity. Additionally, the rotation of the cone also induces a swirl in the fluid, further increasing the tangential velocity. An upsurge in tangential velocity could possess major implications on the distribution of heat and flow behavior of the overall system, and this may prove vital for plenty of engineering applications.

Influence of the magnetic parameter on the tangential velocity profile is plotted in Fig. 4. The variations in M values cause the tangential velocity profile to deteriorate. Whenever an electromagnetic field is directed to a conducting fluid, it contributes to a Lorentz force, which acts perpendicular to both the magnetic field and the fluid velocity. In the case of flow over a cone, this force can act to slow down the tangential velocity of the fluid. The magnetic force can counteract the centrifugal force acting on the fluid, leading to a decrease in the tangential velocity. As the magnetic field strength increases, the magnetic force becomes more significant relative to the centrifugal force, leading to a decrease in the tangential velocity.

Fig. 5 depicts the distinctive features of the nanoparticle volume fraction parameter relative to the tangential velocity profile. The graph shows that higher values of ϕ $(= \phi_{MgO} + \phi_{TiO_2} + \phi_{Al})$ correspond to elevate$f'(y)$.The presence of nanoparticles in the fluid increases the effective viscosity of the fluid, which in turn enhances the momentum transfer between the fluid and the spinning cone. This increased momentum transfer results in a higher tangential velocity of the fluid over the cone. Furthermore, the thermal conductivity of the nanofluid is also higher compared to that of the base fluid, which leads to a faster heat transfer between the cone and the fluid. As a result, the temperature gradient near the cone surface is steeper, which induces a stronger convective flow and increases the tangential velocity of the fluid.

4.2. Discussion on swirl velocity profile

In Fig. 6 it is observed that the swirl velocity of the ternary hybrid nanofluid in all the levels of spin parameter is getting reduced. As said earlier, Fig. 3 evidently reveals that increasing the rotation of the spinning cone generally increases the swirl velocity of the fluid, so it is unlikely that increasing the rotation of the cone would decrease the swirl velocity. The swirl velocity refers to the component of the fluid velocity perpendicular to the axial direction, and it is caused by the tangential velocity of the fluid induced by the spinning motion of the cone. As the cone rotates faster, the fluid near the surface experiences a stronger tangential force, resulting in an increase in the swirl velocity. However,

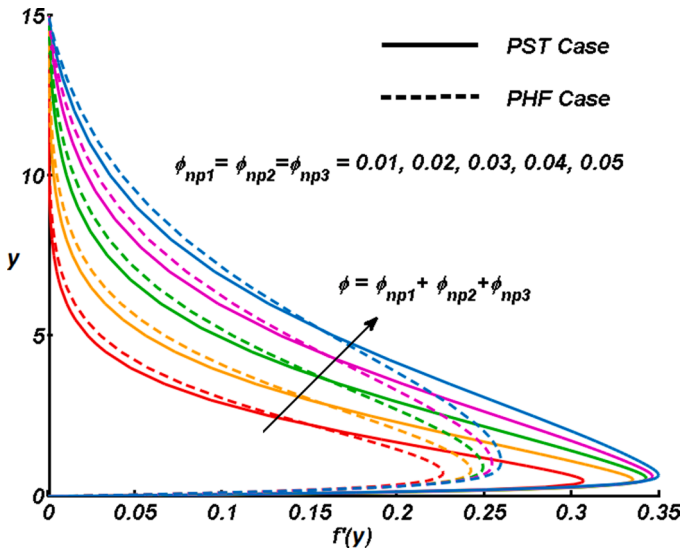

Fig. 5. Influence on tangential velocity by nanoparticle volume fraction parameter.

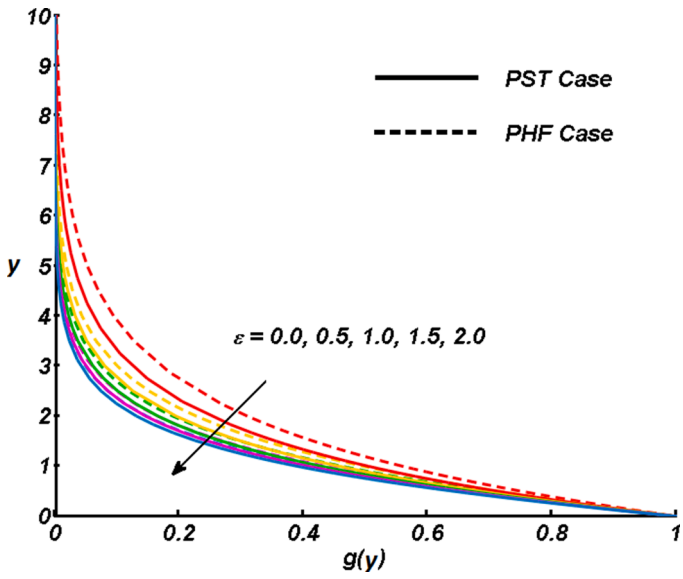

Fig. 6. Influence on swirl velocity by spin parameter.

it is possible that under certain specific conditions, increasing the rotation of the cone might lead to a decrease in swirl velocity. For example, if the fluid viscosity is very high, or if the cone is rotating at a very high speed, the viscous forces or the centrifugal forces may become dominant over the tangential forces, leading to a decrease in swirl velocity. However, such conditions would be rare and not typical in most practical applications.

Fig. 7 highlights the variation of the swirl velocity profile against multiple values of magnetic parameter. From figure, one can notice that$g(y)$ is getting lesser by enhancing the values of M. As discussed earlier in Fig. 4, the Lorentz force results from the interaction between the magnetic field and the electrically conducting fluid, this causes the fluid to experience a force that opposes the direction of flow. In the case of a spinning cone, the swirl velocity is the component of the fluid velocity that is perpendicular to the tangential velocity. The presence of a magnetic field causes the Lorentz force to act on the swirling fluid, which opposes the swirl motion and results in a decrease in the swirl velocity. The magnitude of the Lorentz force depends on the strength of

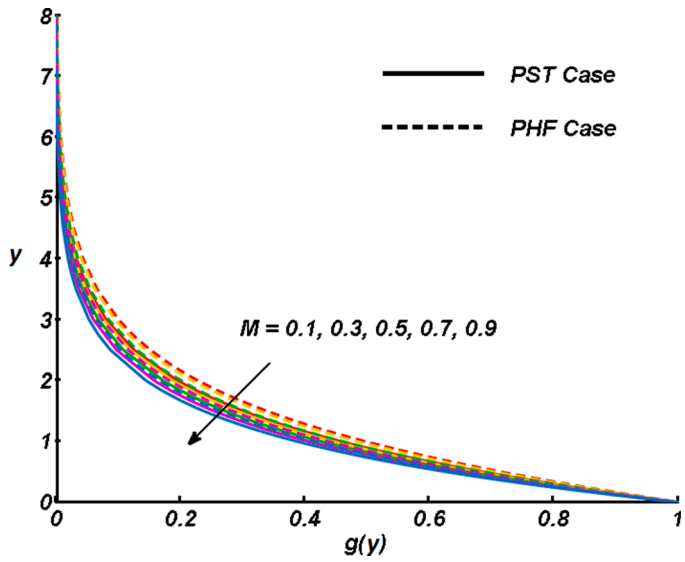

Fig. 7. Influence on swirl velocity by magnetic parameter.

the magnetic field and the electric conductivity of the fluid. In the presence of a strong magnetic field, the Lorentz force can significantly affect the fluid flow, leading to a reduction in the swirl velocity.

In Fig. 8, the swirl velocity profile is plotted to study the impact of nanoparticle volume fraction. When observed, $g(y)$ increases on varying, ϕ $(=\phi_{MgO}+\phi_{TiO_2}+\phi_{Al})$, progressively. As said before, when a temperature gradient is present in a fluid containing nanoparticles (see, Fig. 5), the particles tend to move from regions of high temperature to regions of low temperature due to the thermophoretic effect and from regions of high concentration to regions of low concentration due to the diffusiophoretic effect. This movement can generate vorticity and contribute to the overall swirl velocity of the fluid. In addition to these effects, nanoparticles can also alter the boundary layer thickness or interact with the spinning cone to generate additional vorticity and swirl.

4.3. Discussion on temperature profile

Fig. 9 depicts the impact of spin parameter on the temperature profile. It is clear that $\theta(y)$ reduces for increased values of spin

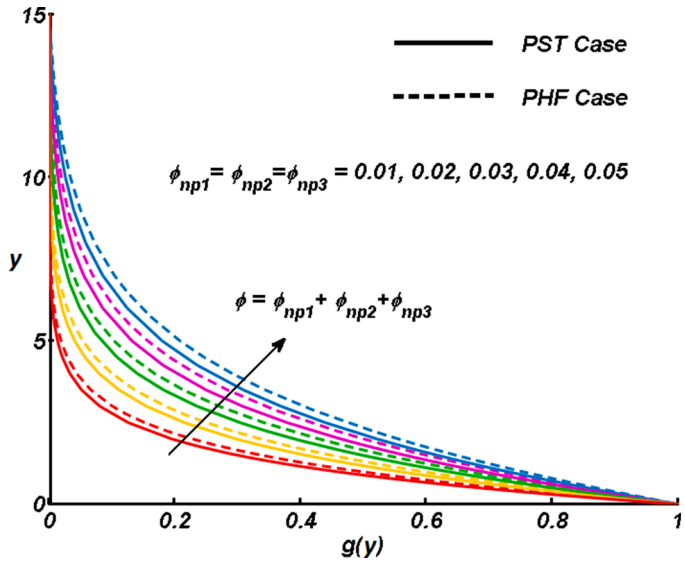

Fig. 8. Influence on swirl velocity by nanoparticle volume fraction parameter.

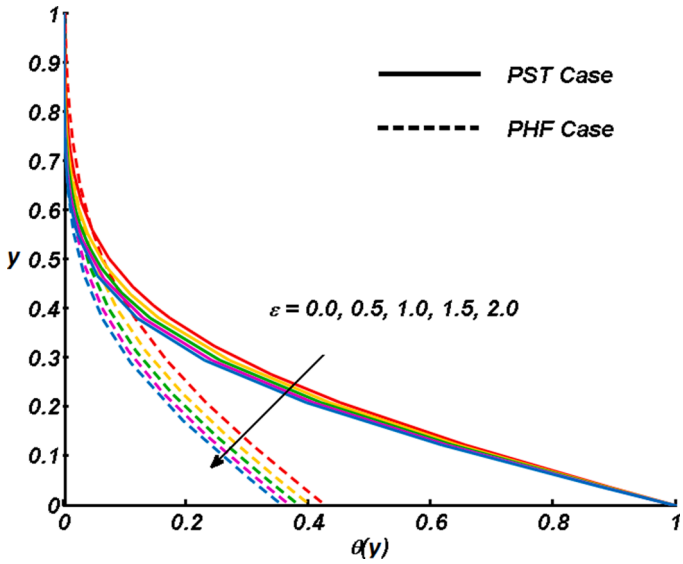

Fig. 9. Influence on temperature profile by spin parameter.

parameter. Increasing the rotation of the spinning cone can decrease the fluid temperature due to the enhanced convective heat transfer caused by the increased fluid velocity. As the spinning cone rotates, it generates a centrifugal force that drives the fluid to move tangentially along the cone surface. This movement can create strong vortices in the fluid, which enhances the convective heat transfer. As the fluid moves faster, the rate of heat transfer from the fluid to the surrounding environment also increases, leading to a decrease in fluid temperature. Furthermore, the increased fluid velocity can also enhance the mixing of the fluid, which can result in a more uniform temperature distribution in the fluid. This can further decrease the average fluid temperature.

The temperature profile over the rotating cone for different values of magnetic parameter is shown in Fig. 10. One can see from the figure that raising the values of M increases$\theta(y)$. When a magnetic field is applied to a conductive fluid, it can induce an electric current in the fluid due to the motion of charged particles under the influence of the Lorentz force. This induced electric current can generate a magnetic field of its own, which interacts with the external magnetic field and creates a force on the fluid, known as the Lorentz force. This Lorentz force can induce a convective flow in the fluid, which can enhance the heat transfer between the fluid and the surrounding environment. As a result, the fluid temperature can increase due to the increased rate of heat transfer from the fluid to the surrounding environment. Moreover, the magnetic field can also influence the thermal conductivity and viscosity of the fluid, which can further affect the convective heat transfer and the fluid temperature.

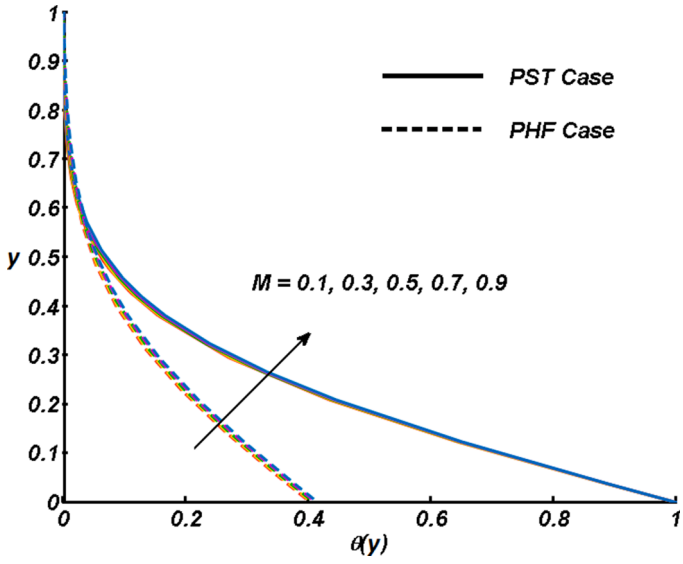

Fig. 10. Influence on temperature profile by magnetic parameter.

For various values of nanoparticle volume fraction the temperature profile is increased as shown in Fig. 11. Nanoparticles have a high surface-to-volume ratio, which makes them efficient heat conductors. When nanoparticles are suspended in a fluid, they can enhance the thermal conductivity of the fluid due to their ability to transfer heat through the inter-particle contacts and the fluid medium. This enhanced thermal conductivity can improve the convective heat transfer between the fluid and the surrounding environment, which can result in an increase in the fluid temperature.

On top of that, a close inspection of Figs. 3, 4, and 5 for the tangential velocity profile and Figs. 9, 10, and 11 for the profile of temperature indicates that the values presented for the PST case are somewhat greater as opposed to the one for the PHF case, regardless of knowing that equivalent developments can be viewed for the two scenarios. This was the unlikely event in Figs. 6, 7, and 8 for swirl velocity.

Figs. 12–15 depict the skin friction coefficient and local Nusselt number for various spin vs. magnetic and spin vs. nanoparticle volume fraction values. The results for M range from 0.1 to 0.9. As observed in the aforementioned graphs, the skin friction coefficient and local Nusselt number of ternary hybrid nanofluids enhance with the spin parameter. On the other hand, enhancing the magnetic parameter leads to modest diminutions in skin friction coefficient and local Nusselt number values for both the PST and PHF cases. In a comparable manner, Figs. 12–15 indicate that in both the PST and PHF cases, the skin friction coefficient and local Nusselt number increased for the nanoparticle volume fraction as each nanoparticle (MgO, TiO_2, and Al) varied from 0.01 to 0.05. The values for the PST mode are also noticeably higher than those for the PHF case.

5. Conclusion

This study emphasizes the importance of taking PST and PHF heating conditions into account when designing and analyzing heat transfer systems based on ternary hybrid nanofluids. At the surface of a rotating cone, swirl flow of ternary hybrid nanofluid of Al, MgO, TiO_2 with water-ethylene glycol was investigated. For the conversion of PDEs into

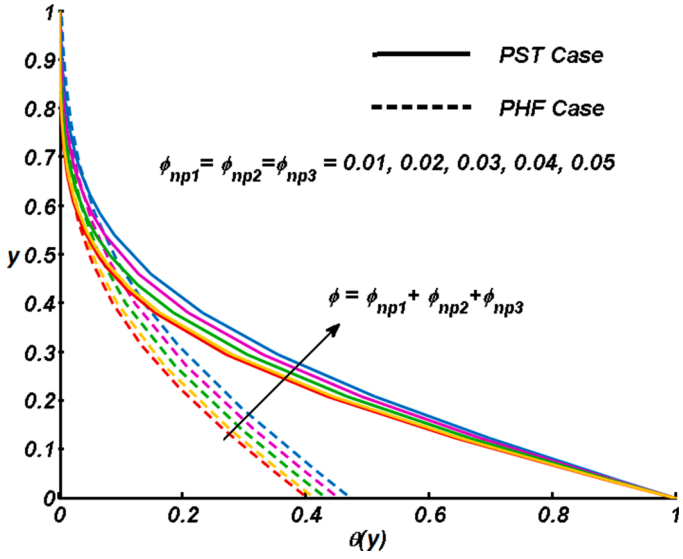

Fig. 11. Influence on temperature profile by nanoparticle volume fraction parameter.

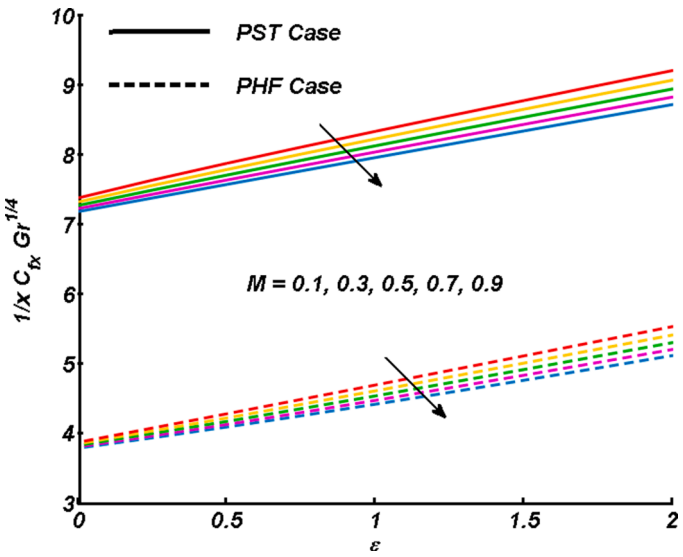

Fig. 12. Influence on the $\frac{1}{x}C_{fx}Gr^{\frac{1}{4}}$ by spin and magnetic parameter.

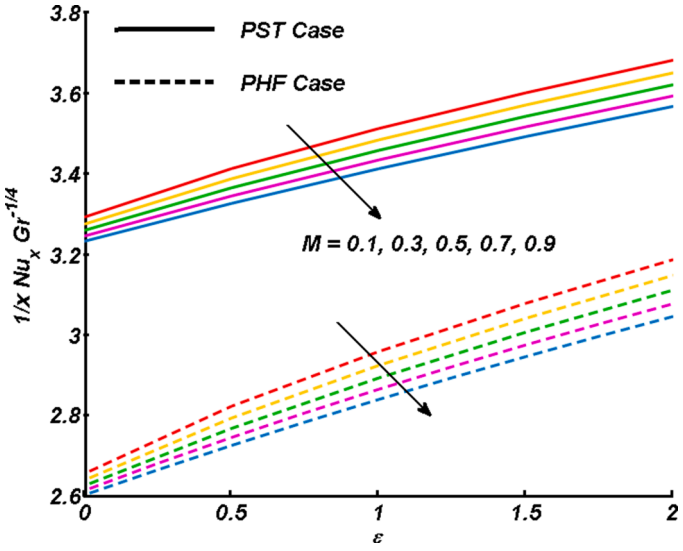

Fig. 13. Influence on $\frac{1}{x}Nu_xGr^{-\frac{1}{4}}$ by spin and magnetic parameter.

ODEs, suitable parameters were considered. By expanding the unknowns and employing the truncated series of shifted Legendre polynomials, numerical solutions were found. The conclusions that follow provide a brief overview of the entire theoretical study.

- Because of the centrifugal force acting on the ternary hybrid nanofluid, increasing the rotation of the spinning cone increases the tangential fluid velocity. The centrifugal forces may become dominant over the tangential forces, resulting in a decrease in swirl velocity.
- Increasing the rotation of the spinning cone can decrease the fluid temperature due to the enhanced convective heat transfer caused by the increased fluid velocity.
- The presence of a magnetic field causes the Lorentz force to act on the swirling ternary hybrid nanofluid, which opposes the tangential and swirl motion and results in a decrease in the tangential and swirl velocity.
- Because of the increased viscosity and thermal conductivity of the nanofluid, increasing the nanoparticle volume fraction generally increases the tangential fluid velocity over a cone.

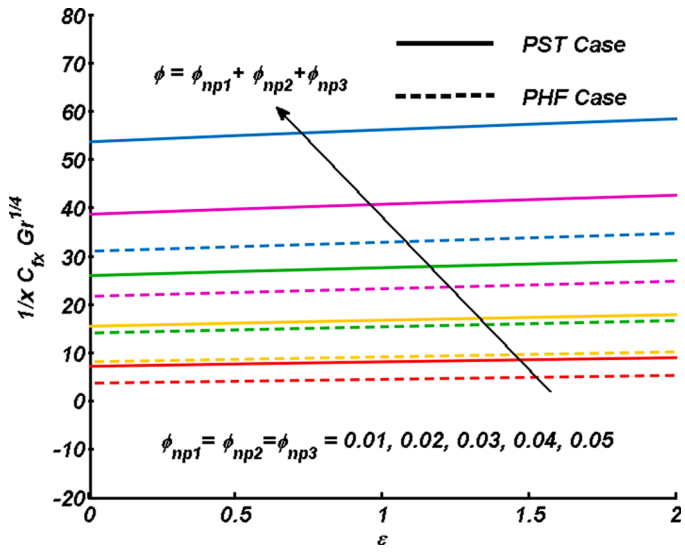

Fig. 14. Influence on $\frac{1}{x}C_{fx}Gr^{\frac{1}{4}}$ by spin and nanoparticle volume fraction parameter.

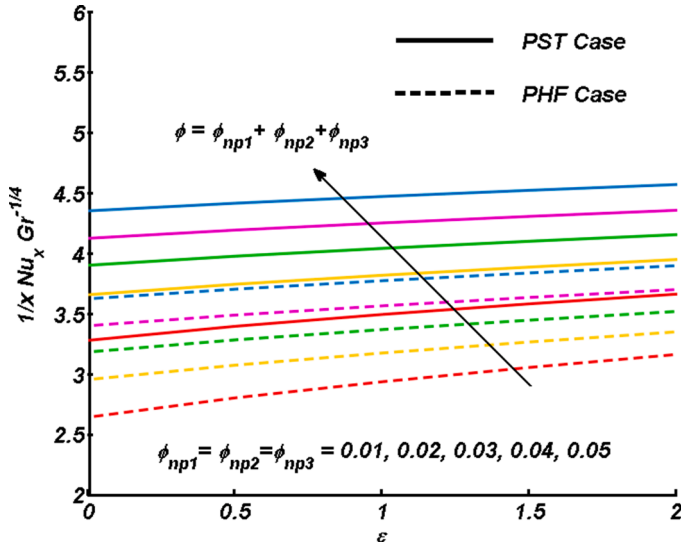

Fig. 15. Influence on $\frac{1}{x}Nu_xGr^{-\frac{1}{4}}$ by spin and nanoparticle volume fraction parameter.

- Nanoparticles in a fluid can induce secondary flows through various mechanisms, such as thermophoresis, diffusiophoresis, and Brownian motion. These secondary flows can alter the overall flow structure and affect the swirl velocity over a cone.
- From all these results it is observed that PST heating condition have a significant impact on the tangential, swirl and temperature profiles.

The ternary hybrid nanofluids should be considered in future research on rotational flows in order to produce nanofluids with extraordinary stability and increased thermal conductivity. The suggested study's findings may play a significant role in a few key industries where better thermal management depends on the flow and heat transfer from spinning cones like: (i) ***Oil Recovery:*** Nanofluids are cutting-edge oil displacement agents with a track record of increased oil recovery effectiveness. Nanofluids have advantages over traditional secondary or tertiary recovery methods such as water flooding or surfactant flooding in terms of high oil recovery, stable differential pressure fluctuation, and a strong nanoparticle breakthrough ability with

minimal formation damage [39]; (ii) ***Bio-Oil:*** Because it is widely available, relatively inexpensive, and emits no harmful gasses, biomass is emerging as the most viable alternative source for manufacturing clean and sustainable goods [40]. Biochemical and thermal conversion techniques can be used to convert biomass into biofuels. Among all of these thermal conversion techniques, fast pyrolysis is regarded as the most promising strategy for producing liquid fuel, such as bio-oil, at its highest potential. Fast pyrolysis is thought to create up to 75% by weight of bio-oil, which can be used directly in a variety of applications or upgraded for use as an energy carrier [41]. A recently developed reactor for pyrolyzing biomass to produce bio-oil with minimal char production is the spinning cone reactor.

Declaration of Competing Interest

The authors declare the following financial interests/personal relationships which may be considered as potential competing interests:

Saranya Shekar reports was provided by United Arab Emirates University. Saranya Shekar reports a relationship with United Arab Emirates University that includes: employment.

Data availability

No data was used for the research described in the article.

Acknowledgements

The authors would like to thank the United Arab Emirates University, Al Ain, UAE for providing financial support through SDGs Research Program 2023 and SURE Plus 2023.

Appendix 1

The coefficients in Eqns. (9)-(11) are given as follows (for more details see: Sahoo [1] and Xiu et al. [37]):

$$k_{Thnf} = \frac{k_{nf1}\phi_{Al} + k_{nf2}\phi_{TiO_2} + k_{nf3}\phi_{MgO}}{\phi}, \quad \mu_{Thnf} = \frac{\mu_{nf1}\phi_{Al} + \mu_{nf2}\phi_{TiO_2} + \mu_{nf3}\phi_{MgO}}{\phi},$$

$$\rho_{Thnf} = (1 - \phi_{MgO} - \phi_{TiO_2} - \phi_{Al})\rho_{bf} + \phi_{MgO}\rho_{MgO} + \phi_{TiO_2}\rho_{TiO_2} + \phi_{Al}\rho_{Al},$$

$$\beta_{Thnf} = (1 - \phi_{MgO} - \phi_{TiO_2} - \phi_{Al})\beta_{bf} + \phi_{MgO}\beta_{MgO} + \phi_{TiO_2}\beta_{TiO_2} + \phi_{Al}\beta_{Al},$$

$$(\rho Cp)_{Thnf} = (1 - \phi_{MgO} - \phi_{TiO_2} - \phi_{Al})(\rho Cp)_{bf} + \phi_{MgO}(\rho Cp)_{MgO} + \phi_{TiO_2}(\rho Cp)_{TiO_2} + \phi_{Al}(\rho Cp)_{Al},$$

$$\phi = \phi_{MgO} + \phi_{TiO_2} + \phi_{Al}$$

$$k_{nf1} = k_{bf}\left[\frac{-2\phi_{Al}(k_{bf} - k_{Al}) + 2k_{bf} + k_{Al}}{\phi_{Al}(k_{bf} - k_{Al}) + 2k_{bf} + k_{Al}}\right],$$

$$k_{nf2} = k_{bf}\left[\frac{-3.9\phi_{TiO_2}(k_{bf} - k_{TiO_2}) + 3.9k_{bf} + k_{TiO_2}}{\phi_{TiO_2}(k_{bf} - k_{TiO_2}) + 3.9k_{bf} + k_{TiO_2}}\right],$$

$$k_{nf3} = k_{bf}\left[\frac{-4.7\phi_{MgO}(k_{bf} - k_{MgO}) + 4.7k_{bf} + k_{MgO}}{\phi_{MgO}(k_{bf} - k_{MgO}) + 4.7k_{bf} + k_{MgO}}\right],$$

$$\mu_{nf1} = (6.2\phi^2 + 2.5\phi + 1)\mu_{bf},$$

$$\mu_{nf2} = (904.4\phi^2 + 13.5\phi + 1)\mu_{bf},$$

$$\mu_{nf3} = (612.6\phi^2 + 37.1\phi + 1)\mu_{bf},$$

$$C_1 = 6.2\phi^2 + 2.5\phi + 1,$$

$$C_2 = 904.4\phi^2 + 13.5\phi + 1,$$

$$C_3 = 612.6\phi^2 + 37.1\phi + 1,$$

$$C_4 = C_1\phi_{MgO} + C_2\phi_{TiO_2} + C_3\phi_{Al},$$

$$C_5 = (1 - \phi_{MgO} - \phi_{TiO_2} - \phi_{Al}) + \frac{\phi_{MgO}\rho_{MgO}}{\rho_{bf}} + \frac{\phi_{TiO_2}\rho_{TiO_2}}{\rho_{bf}} + \frac{\phi_{Al}\rho_{Al}}{\rho_{bf}},$$

$$C_6 = \frac{-2\phi_{Al}(k_{bf} - k_{Al}) + 2k_{bf} + k_{Al}}{\phi_{Al}(k_{bf} - k_{Al}) + 2k_{bf} + k_{Al}},$$

$$C_7 = \frac{-3.9\phi_{TiO_2}(k_{bf} - k_{TiO_2}) + 3.9k_{bf} + k_{TiO_2}}{\phi_{TiO_2}(k_{bf} - k_{TiO_2}) + 3.9k_{bf} + k_{TiO_2}},$$

$$C_8 = \frac{-4.7\phi_{MgO}(k_{bf} - k_{MgO}) + 4.7k_{bf} + k_{MgO}}{\phi_{MgO}(k_{bf} - k_{MgO}) + 4.7k_{bf} + k_{MgO}},$$

$$C_9 = (1 - \phi_{MgO} - \phi_{TiO_2} - \phi_{Al}) + \frac{\phi_{MgO}(\rho Cp)_{MgO}}{(\rho Cp)_{bf}} + \frac{\phi_{TiO_2}(\rho Cp)_{TiO_2}}{(\rho Cp)_{bf}} + \frac{\phi_{Al}(\rho Cp)_{Al}}{(\rho Cp)_{bf}},$$

$$C_{10} = C_6\phi_{MgO} + C_7\phi_{TiO_2} + C_8\phi_{Al}.$$

$$C_{11} = (1 - \phi_{MgO} - \phi_{TiO_2} - \phi_{Al}) + \frac{\phi_{MgO}\beta_{MgO}}{\beta_{bf}} + \frac{\phi_{TiO_2}\beta_{TiO_2}}{\beta_{bf}} + \frac{\phi_{Al}\beta_{Al}}{\beta_{bf}},$$

References

[1] R.R. Sahoo, Thermo-hydraulic characteristics of radiator with various shape nanoparticle-based ternary hybrid nanofluid, Powder Technol. 370 (2020) 19–28.
[2] W. Cao, I.L. Animasaun, S.J. Yook, V.A. Oladipupo, X. Ji, Simulation of the dynamics of colloidal mixture of water with various nanoparticles at different levels of partial slip: ternary-hybrid nanofluid, Int. Commun. Heat Mass Transf. 135 (2022) p.106069.
[3] Z. Said, N.K. Cakmak, P. Sharma, L.S. Sundar, A. Inayat, O. Keklikcioglu, C. Li, Synthesis, stability, density, viscosity of ethylene glycol-based ternary hybrid nanofluids: experimental investigations and model-prediction using modern machine learning techniques, Powder Technol. 400 (2022) p.117190.
[4] H. Adun, M. Adedeji, M. Dagbasi, A. Babatunde, Amelioration of thermodynamic performance and environmental analysis of an integrated solar power generation system with storage capacities using optimized ternary hybrid nanofluids, J. Energy Storage 51 (2022) p.104531.
[5] Y. Shao, M.K. Nayak, A.S. Dogonchi, A.J. Chamkha, Y. Elmasry, A.M. Galal, Ternary hybrid nanofluid natural convection within a porous prismatic enclosure with two movable hot baffles: an approach to effective cooling, Case Stud. Therm. Eng. 40 (2022) p.102507.
[6] I. Shahzadi, F.Z. Duraihem, S. Ijaz, C.S.K. Raju, S. Saleem, Blood stream alternations by mean of electroosmotic forces of fractional ternary nanofluid through the oblique stenosed aneurysmal artery with slip conditions, Int. Commun. Heat Mass Transf. 143 (2023) p.106679.
[7] X. Wang, Q. Wen, J. Yang, S. Shittu, X. Wang, X. Zhao, Z. Wang, Heat transfer and flow characteristic of a flat confined loop thermosyphon with ternary hybrid nanofluids for electronic devices cooling, Appl. Therm. Eng. 221 (2023) p.119758.
[8] I.L. Animasaun, Q.M. Al-Mdallal, U. Khan, A.S. Alshomrani, Unsteady water-based ternary hybrid nanofluids on wedges by bioconvection and wall stretching velocity: thermal analysis and scrutinization of small and larger magnitudes of the thermal conductivity of nanoparticles, Mathematics 10 (22) (2022) p.4309.
[9] M. Arif, P. Kumam, W. Kumam, Z. Mostafa, Heat transfer analysis of radiator using different shaped nanoparticles water-based ternary hybrid nanofluid with applications: a fractional model, Case Stud. Therm. Eng. 31 (2022) p.101837.
[10] K. Sarada, F. Gamaoun, A. Abdulrahman, S.O. Paramesh, R. Kumar, G.D. Prasanna, R.P. Gowda, Impact of exponential form of internal heat generation on water-based ternary hybrid nanofluid flow by capitalizing non-Fourier heat flux model, Case Stud. Therm. Eng. 38 (2022) p.102332.
[11] A. Boroomandpour, D. Toghraie, M. Hashemian, A comprehensive experimental investigation of thermal conductivity of a ternary hybrid nanofluid containing MWCNTs-titania-zinc oxide/water-ethylene glycol (80: 20) as well as binary and mono nanofluids, Synth. Met. 268 (2020) p.116501.
[12] C.L. Tien, D.T. Campbell, Heat and mass transfer from rotating cones, J. Fluid Mech. 17 (1) (1963) 105–112.
[13] R. Banerjee, M. Rout, A. Karmakar, D. Bose, Free vibration response of rotating hybrid composite conical shell under hygrothermal conditions, J. Vib. Eng. Technol. (2022) 1–18.
[14] P.C. Riley, S.J. Sykes, Industrial applications of spinning cone column technology: a review, Distillation Absorption 1 (2002) 1–15.
[15] F.J. Cloos, P. Pelz, December. Swirl boundary layer at the inlet of a rotating circular cone, in: 17th International Symposium on Transport Phenomena and Dynamics of Rotating Machinery (ISROMAC2017), 2017.
[16] H. Guoxin, G. Xiwu, H. Hao, F. Haojie, W. Zheng, Experimental studies on flow and pyrolysis of coal with solid heat carrier in a modified rotating cone reactor, Chem. Eng. Process.: Process Intensification 47 (9–10) (2008) 1777–1785.
[17] B.M. Wagenaar, W. Prins, W.P.M. Van Swaaij, Pyrolysis of biomass in the rotating cone reactor: modelling and experimental justification, Chem. Eng. Sci. 49 (24) (1994) 5109–5126.
[18] R.W.J. Westerhout, J. Waanders, J.A.M. Kuipers, W.P.M. van Swaaij, Development of a continuous rotating cone reactor pilot plant for the pyrolysis of polyethene and polypropene, Ind. Eng. Chem. Res. 37 (6) (1998) 2316–2322.
[19] M.J. MacDonald, S.J. Muller, Experimental study of shear-induced migration of polymers in dilute solutions, J. Rheol. (N Y N Y) 40 (2) (1996) 259–283.
[20] A.M. Janse, P.M. Biesheuvel, W. Prins, W.P. van Swaaij, Granular flow in a rotating cone partly submerged in a fluidized bed, AIChE J. 46 (3) (2000) 499–508.
[21] F. Kreith, D. Ellis, J. Giesing, An experimental investigation of the flow engendered by a rotating cone, Appl. Sci. Res., Section A, 11 (1963) 430–440.
[22] S. Saranya, L. Baranyi, Q.M. Al-Mdallal, Free convection flow of hybrid ferrofluid past a heated spinning cone, Therm. Sci. Eng. Prog. 32 (2022) p.101335.
[23] A.A. Hakeem, S. Kirusakthika, B. Ganga, M. Ijaz Khan, M.K. Nayak, T. Muhammad, S.U. Khan, Transverse magnetic effects of hybrid nanofluid flow over a vertical rotating cone with Newtonian/non-Newtonian base fluids, in: Waves in Random and Complex Media, 2021, pp. 1–18.
[24] A.R. Mogharrebi, D. Ganji, A.R. Hosseinzadeh, Roghani K, Asadi, A S, A. Fazlollahtabar, Investigation of magnetohydrodynamic nanofluid flow contain motile oxytactic microorganisms over rotating cone, Int. J. Numer. Methods Heat Fluid Flow 31 (11) (2021) 3394–3412.
[25] P. Rana, G. Gupta, FEM solution to quadratic convective and radiative flow of Ag-MgO/H2O hybrid nanofluid over a rotating cone with Hall current: optimization using response surface methodology, Math. Comput. Simul. 201 (2022) 121–140.
[26] S.A. Khan, T. Hayat, M.I. Khan, A. Alsaedi, Salient features of Dufour and Soret effect in radiative MHD flow of viscous fluid by a rotating cone with entropy generation, Int. J. Hydrogen Energy 45 (28) (2020) 14552–14564.
[27] A. Hussain, A. Hassan, M. Arshad, A. Rehman, R.T. Matoog, T. Abdeljawad, Numerical simulation and thermal enhancement of multi-based nanofluid over an embrittled cone, Case Stud. Therm. Eng. 28 (2021) p.101614.
[28] U. Nazir, M. Sohail, M.M. Selim, H. Alrabaiah, P. Kumam, Finite element simulations of hybrid nano-Carreau Yasuda fluid with hall and ion slip forces over rotating heated porous cone, Sci. Rep. 11 (1) (2021) p.19604.
[29] H.A. Nabwey, A. Mahdy, Transient flow of micropolar dusty hybrid nanofluid loaded with Fe3O4-Ag nanoparticles through a porous stretching sheet, Results Phys. 21 (2021) p.103777.
[30] M.R. Eid, F. Mabood, Entropy analysis of a hydromagnetic micropolar dusty carbon NTs-kerosene nanofluid with heat generation: Darcy–Forchheimer scheme, J. Therm. Anal. Calorim. 143 (3) (2021) 2419–2436.
[31] I. Ahmad, M. Faisal, T. Javed, A. Mustafa, M.Z. Kiyani, Numerical investigation for mixed convective 3D radiative flow of chemically reactive Williamson nanofluid with power law heat/mass fluxes, Ain Shams Eng. J. 13 (1) (2022) p.101508.
[32] A. Mostafazadeh, D. Toghraie, R. Mashayekhi, O.A. Akbari, Effect of radiation on laminar natural convection of nanofluid in a vertical channel with single-and two-phase approaches, J. Therm. Anal. Calorim. 138 (1) (2019) 779–794.
[33] I. Ahmad, Q. Zan-Ul-Abadin, M. Faisal, K. Loganathan, T. Javed, D.K. Chaudhary, Prescribed thermal activity in the radiative bidirectional flow of magnetized hybrid nanofluid: Keller-Box approach, J. Nanomaterials (2022) 2022.
[34] D. Bhukta, G.C. Dash, S.R. Mishra, S. Jena, Analytical estimation of energy dissipations: viscous, Joulian, and Darcy of viscoelastic fluid flow phenomena over a deformable surface, Heat Transf. 50 (8) (2021) 7798–7816.
[35] M.C. Ece, Free convection flow about a vertical spinning cone under a magnetic field, Appl. Math. Comput. 179 (1) (2006) 231–242.
[36] M. Aghamajidi, M. Yazdi, S. Dinarvand, I. Pop, Tiwari-Das nanofluid model for magnetohydrodynamics (MHD) natural-convective flow of a nanofluid adjacent to a spinning down-pointing vertical cone, Propuls. Power Res. 7 (1) (2018) 78–90.
[37] W. Xiu, I.L. Animasaun, Q.M. Al-Mdallal, A.K. Alzahrani, T. Muhammad, Dynamics of ternary-hybrid nanofluids due to dual stretching on wedge surfaces when volume of nanoparticles is small and large: forced convection of water at different temperatures, Int. Commun. Heat Mass Transf. 137 (2022) p.106241.
[38] S. Saranya, Q.M. Al-Mdallal, S. Javed, Shifted legendre collocation method for the solution of unsteady viscous-ohmic dissipative hybrid ferrofluid flow over a cylinder, Nanomaterials 11 (6) (2021) p.1512.
[39] W.H. Yao, L. Yu, Experiment research on flooding by nano-solution in Jiangsu oil field, Petrochem. Ind. Appl. 30 (1) (2011) 8–12.
[40] S. Li, S. Xu, S. Liu, C. Yang, Q. Lu, Fast pyrolysis of biomass in free-fall reactor for hydrogen-rich gas, Fuel Process. Technol. 85 (8–10) (2004) 1201–1211.
[41] S. Czernik, A.V. Bridgwater, Overview of applications of biomass fast pyrolysis oil, Energy Fuels 18 (2) (2004) 590–598.